

## Supporting Information

### Dual-enzyme decorated semiconducting polymer nanoagents for second near-infrared photoactivatable ferroptosis-immunotherapy

Yue Liu,<sup>‡a</sup> Renjie Lu,<sup>‡b</sup> Meng Li,<sup>a</sup> Danling Cheng,<sup>a</sup> Fengshuo Wang,<sup>a</sup> Xiumei Ouyang,<sup>c</sup> Yitian Zhang,<sup>c</sup>

Qin Zhang,<sup>\*d</sup> Jingchao Li<sup>\*a</sup> and Shaojun Peng<sup>\*c</sup>

<sup>a</sup> State Key Laboratory for Modification of Chemical Fibers and Polymer Materials, Shanghai Engineering Research Center of Nano-Biomaterials and Regenerative Medicine, College of Biological Science and Medical Engineering, Donghua University, Shanghai 201620, China. E-mail: [jcli@dhu.edu.cn](mailto:jcli@dhu.edu.cn)

<sup>b</sup> Department of Orthopedics, Shanghai Sixth People's Hospital Affiliated to Shanghai Jiao Tong University School of Medicine, Shanghai 200233, China.

<sup>c</sup> Zhuhai Institute of Translational Medicine, Zhuhai Precision Medical Center, Zhuhai People's Hospital (Zhuhai hospital affiliated with Jinan University), Zhuhai, Guangdong 519000, China. Email: [henry2008\\_ok@126.com](mailto:henry2008_ok@126.com)

<sup>d</sup> Institute of Translational Medicine, Shanghai University, Shanghai 200444, China. Email: [Sabrina\\_1985@shu.edu.cn](mailto:Sabrina_1985@shu.edu.cn)

<sup>‡</sup> These authors contributed equally to this work.

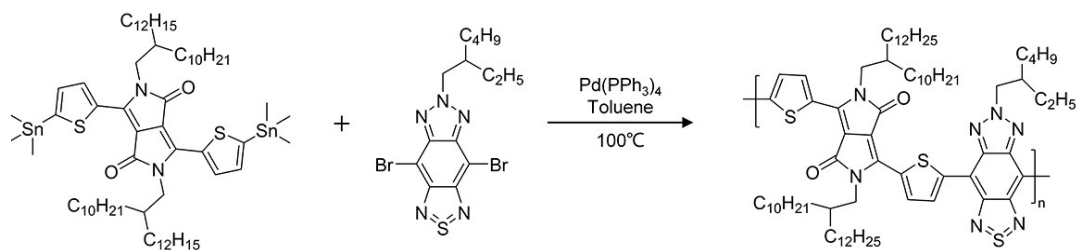


**Fig. S1.** Schematic of the synthetic routes of SP.

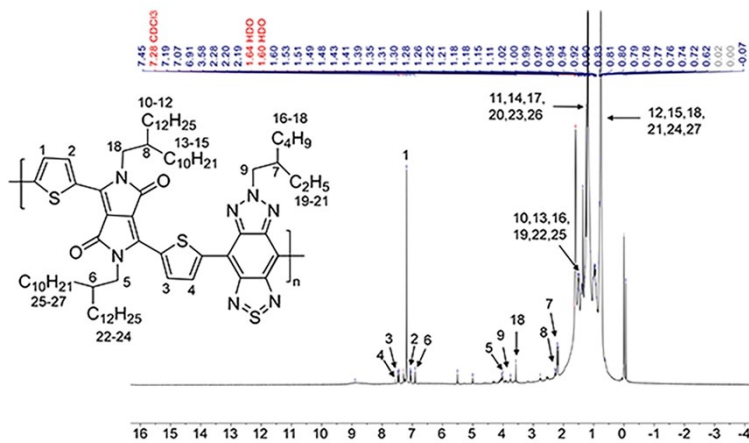


**Fig. S2.** <sup>1</sup>H NMR spectrum of SP in CDCl<sub>3</sub>-D.

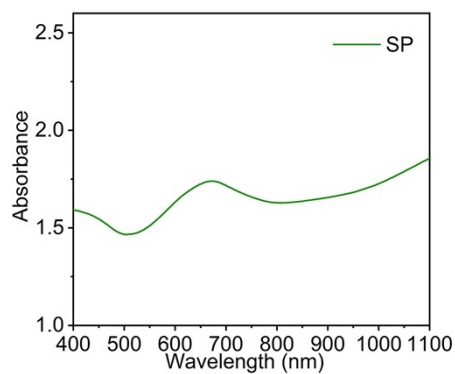


**Fig. S3.** Absorbance spectrum of SP (100 µg/mL).

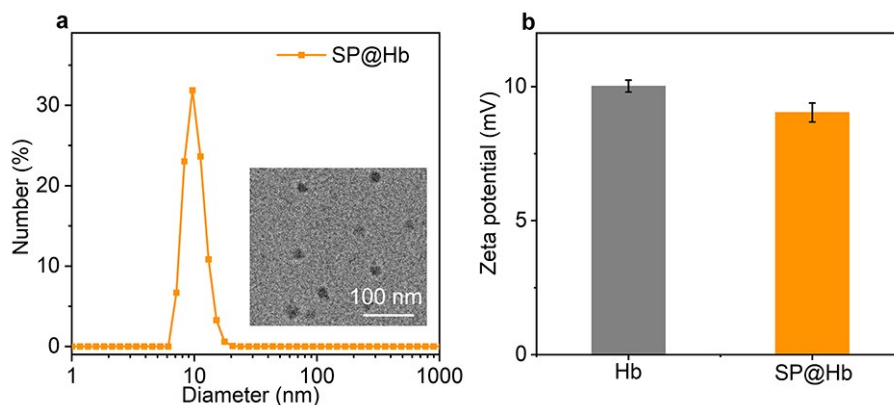


**Fig. S4.** (a) TEM image and hydrodynamic size of SP@Hb (5 µg/mL). (b) Zeta potentials of Hb and SP@Hb (5 µg/mL) (n = 5).

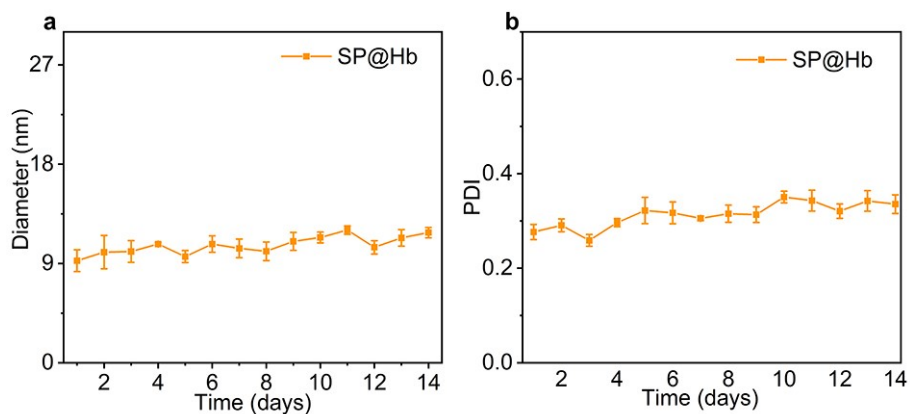


**Fig. S5.** (a) Hydrodynamic sizes of SP@Hb on different days in PBS (5 µg/mL) (n = 5). (b) PDI of SP@Hb on different days in PBS solution (5 µg/mL) (n = 5).

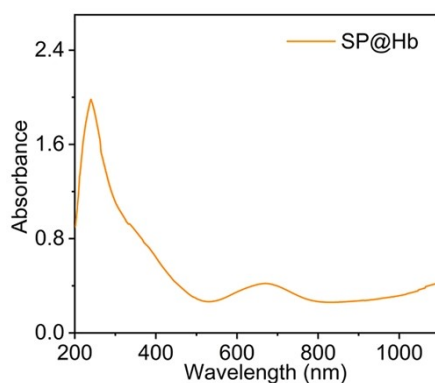


**Fig. S6.** Absorbance spectrum of SP@Hb (20 µg/mL).

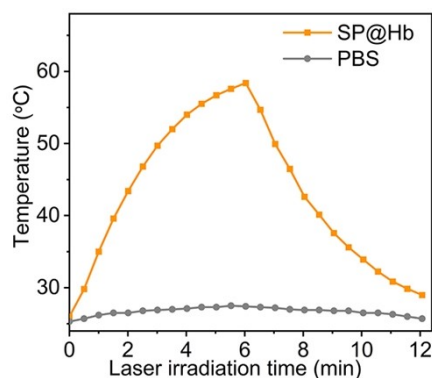


**Fig. S7.** Temperature curves of SP@Hb (100 µg/mL) and PBS solution under 1064 nm laser irradiation.

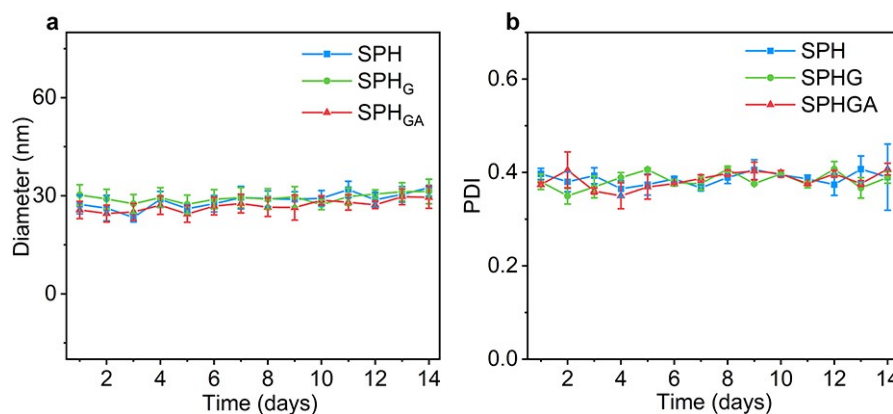


**Fig. S8.** (a) Hydrodynamic sizes of SPH, SPH<sub>G</sub>, and SPH<sub>GA</sub> on different days in PBS solution (5 μg/mL) (n = 5). (b) PDI of SPH, SPH<sub>G</sub>, and SPH<sub>GA</sub> on different days in PBS solution (5 μg/mL) (n = 5).

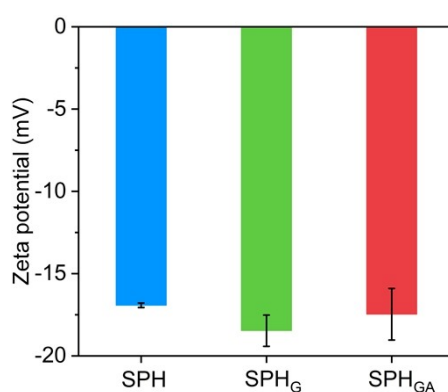


**Fig. S9.** Zeta potential measurements of SPH, SPH<sub>G</sub> and SPH<sub>GA</sub> (5 μg/mL) (n = 5).

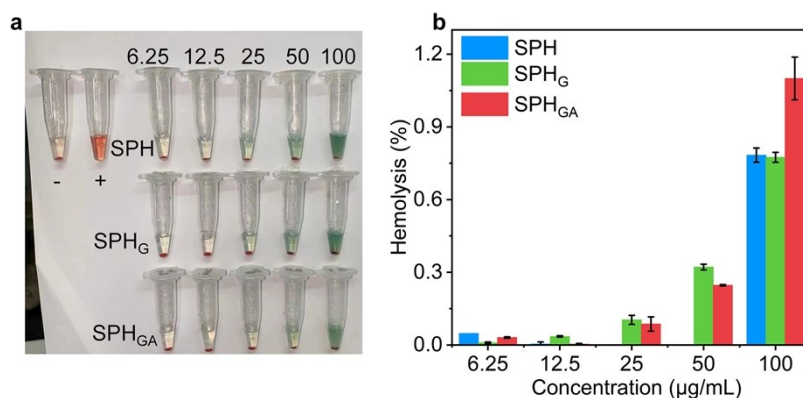


**Fig. S10.** (a) Hemolysis analysis of blood red cells after incubations with SPH, SPH<sub>G</sub> and SPH<sub>GA</sub> at different concentrations for 2 h. (b) Hemolysis percentages of blood red cells after treatments (n = 3).

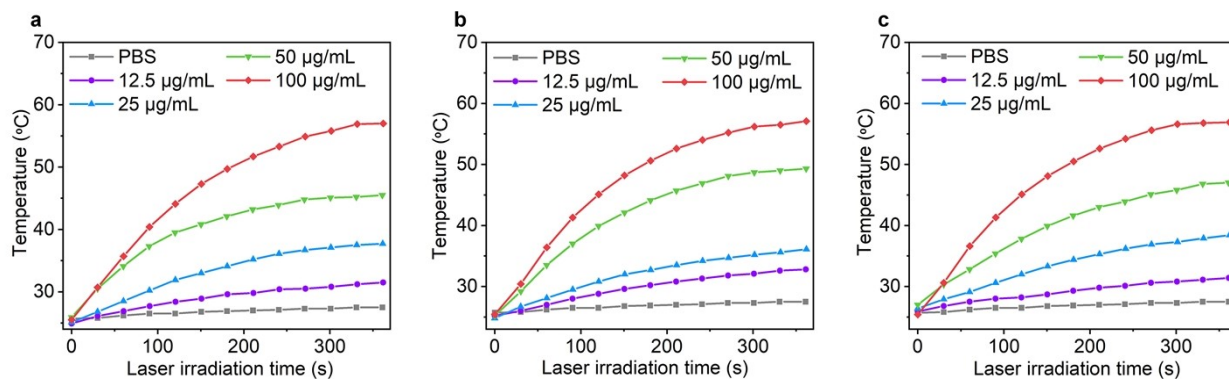


**Fig. S11.** Temperature change curves of (a) SPH, (b) SPH<sub>G</sub> and (c) SPH<sub>GA</sub> at different concentrations under 1064 nm laser irradiation.

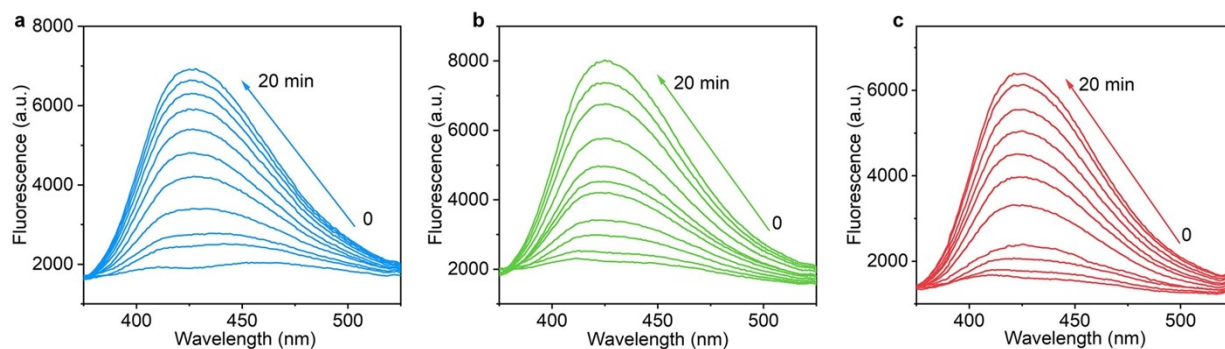


**Fig. S12.** Fluorescence intensity of ·OH probe for (a) SPH, (b) SPH<sub>G</sub> and (c) SPH<sub>GA</sub> under 1064 nm laser irradiation for different times (25 µg/mL).

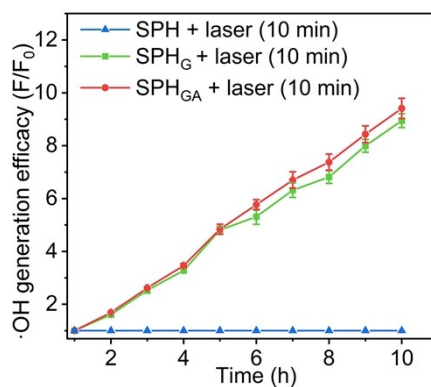


**Fig. S13.** Evaluation of ·OH generation for SPH, SPH<sub>G</sub> and SPH<sub>GA</sub> (150 µg/mL) after 10 min of 1064 nm laser irradiation at different incubation time (n = 3).

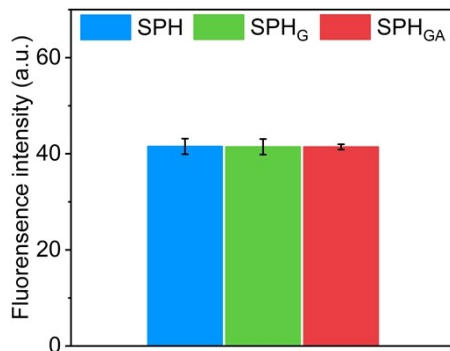


**Fig. S14.** Mean fluorescence intensity of red signals for SPH-, SPH<sub>G</sub>- and SPH<sub>GA</sub>-treated cells (15 µg/mL) (n = 5).

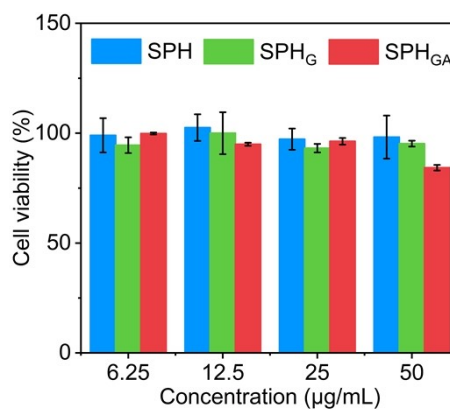


**Fig. S15.** Cell viability analysis of SPH-, SPH<sub>G</sub>- and SPH<sub>GA</sub>-treated 4T1 cells (n = 5).

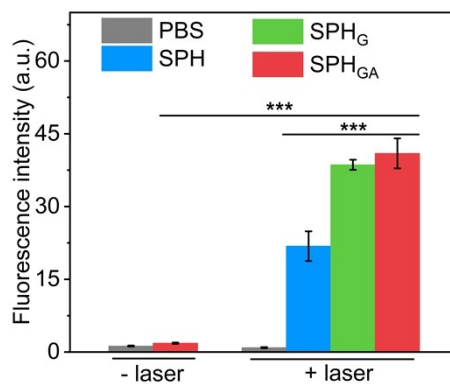


**Fig. S16.** Fluorescence intensity of the generated ·OH for various treated 4T1 cells (25 µg/mL) (n = 5).

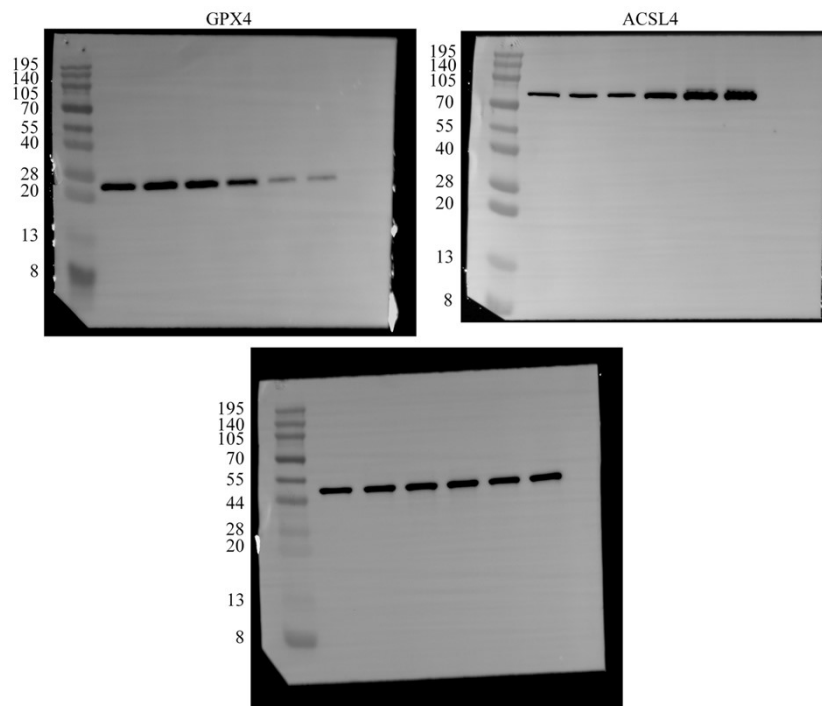


**Fig. S17.** The uncropped Western blot for Fig 3f.

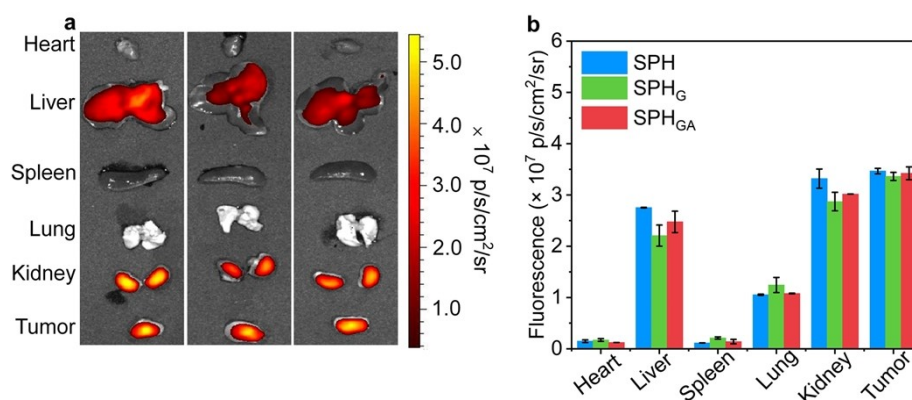


**Fig. S18.** (a) Fluorescence imaging of tumors, livers, kidneys, spleens, lungs and hearts. (b) Analysis of fluorescence intensity of major tissues (250  $\mu\text{g}/\text{mL}$ , 200  $\mu\text{L}$ ) ( $n = 3$ ).

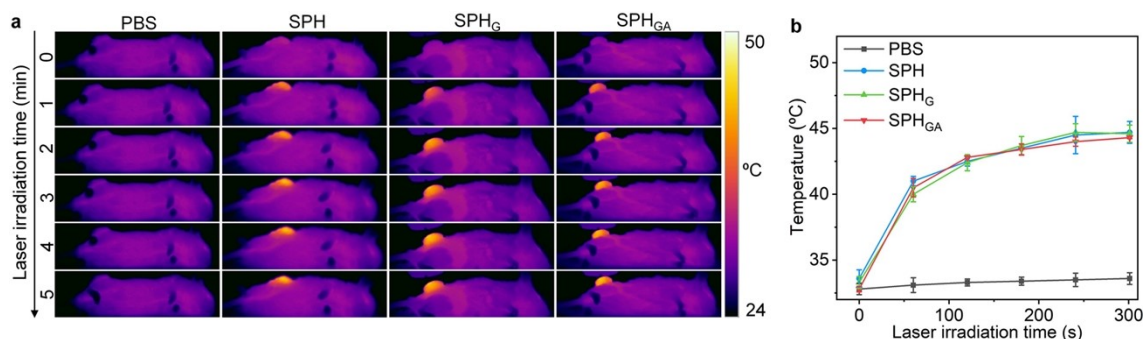


**Fig. S19.** (a) Thermal imaging of tumor-bearing mice under irradiation of the tumors using 1064 nm laser. (b) Temperature change curves of tumors after injection of nanoparticles (250  $\mu\text{g}/\text{mL}$ , 200  $\mu\text{L}$ ) under laser irradiation (1.0  $\text{W}/\text{cm}^2$ , 5 min) ( $n = 3$ ).



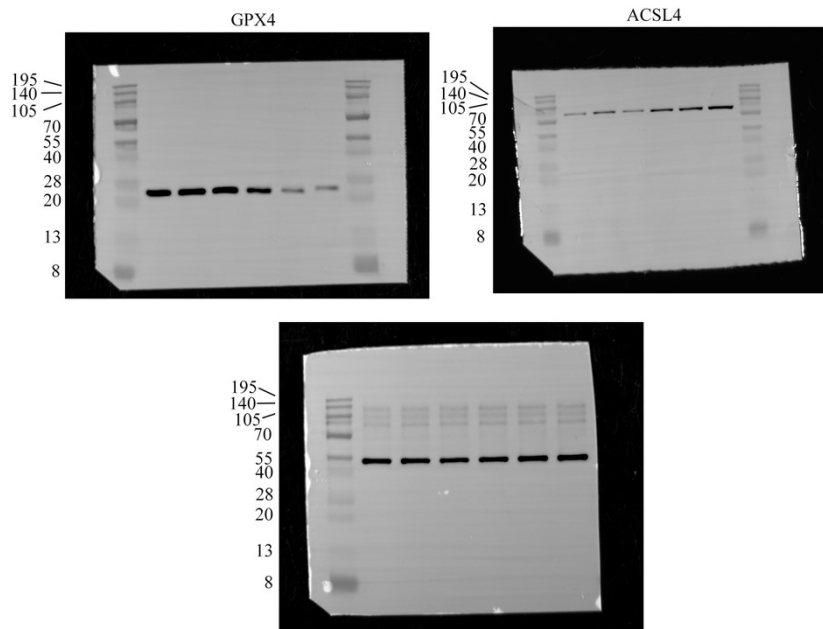


**Fig. S20.** The uncropped Western blot for Fig 5c.

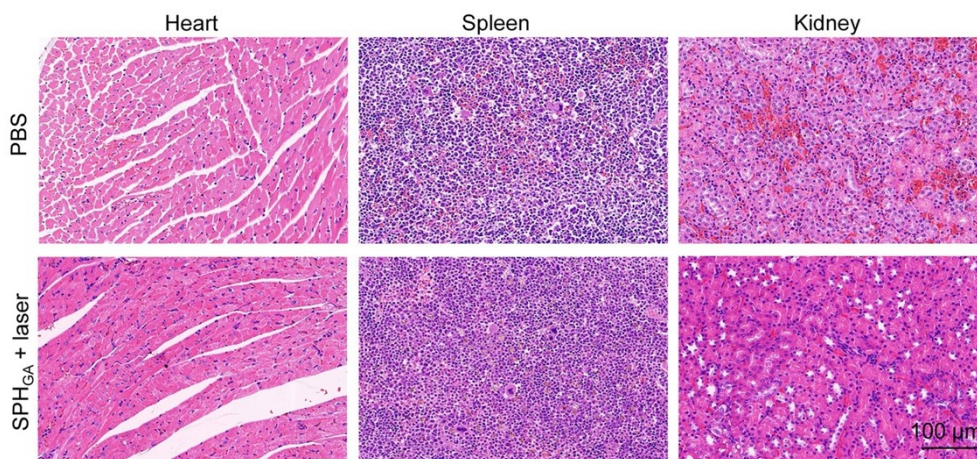


**Fig. S21.** H&E staining images of heart, spleen and kidney in PBS and SPH<sub>GA</sub> + laser groups (250 μg/mL, 200 μL).

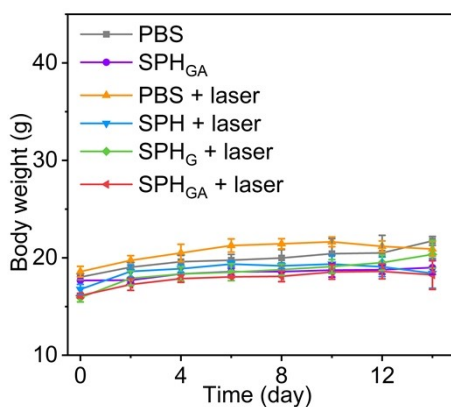


**Fig. S22.** Body weights of tumor-bearing mice after treatments with PBS, SPH, SPH<sub>G</sub> and SPH<sub>GA</sub> (250 μg/mL, 200 μL) and laser irradiation (1.0 W/cm<sup>2</sup>, 10 min) (n = 5).



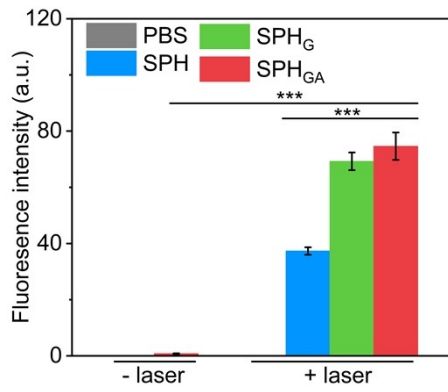


**Fig. S23.** Mean fluorescence intensity of CRT staining signals of primary tumors after treatments with SPH, SPH<sub>G</sub> and SPH<sub>GA</sub> (250 µg/mL, 200 µL) and laser irradiation (1.0 W/cm<sup>2</sup>, 10 min) (n = 5).

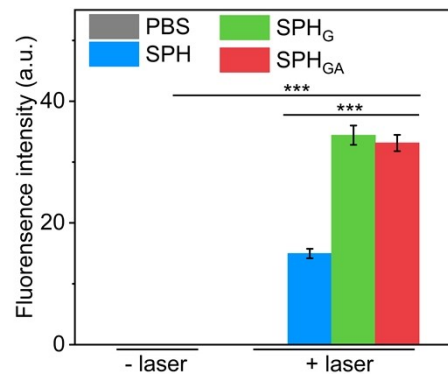


**Fig. S24.** Mean fluorescence intensity of HMGB1 staining signals of primary tumors after treatments with SPH, SPH<sub>G</sub> and SPH<sub>GA</sub> (250 µg/mL, 200 µL) and laser irradiation (1.0 W/cm<sup>2</sup>, 10 min) (n = 5).

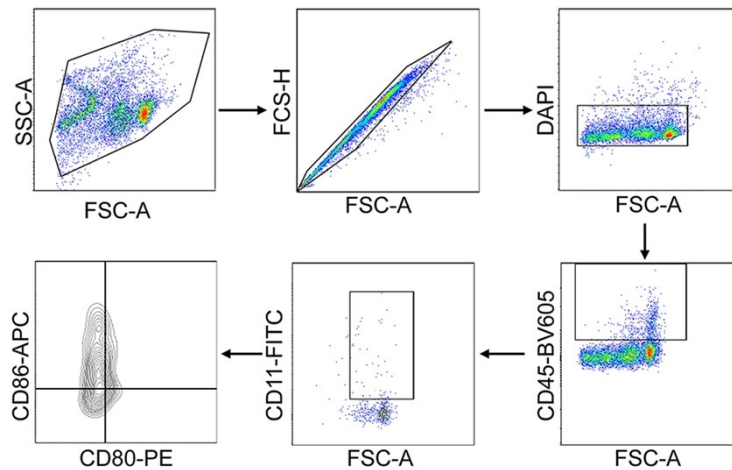


**Fig. S25.** Gating strategy for flow cytometry analysis of matured DCs (CD80<sup>+</sup>CD86<sup>+</sup>).

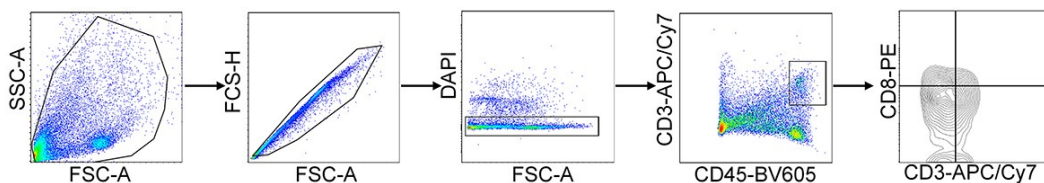


**Fig. S26.** Gating strategy for flow cytometry analysis of matured CD3<sup>+</sup>CD8<sup>+</sup> T cells.

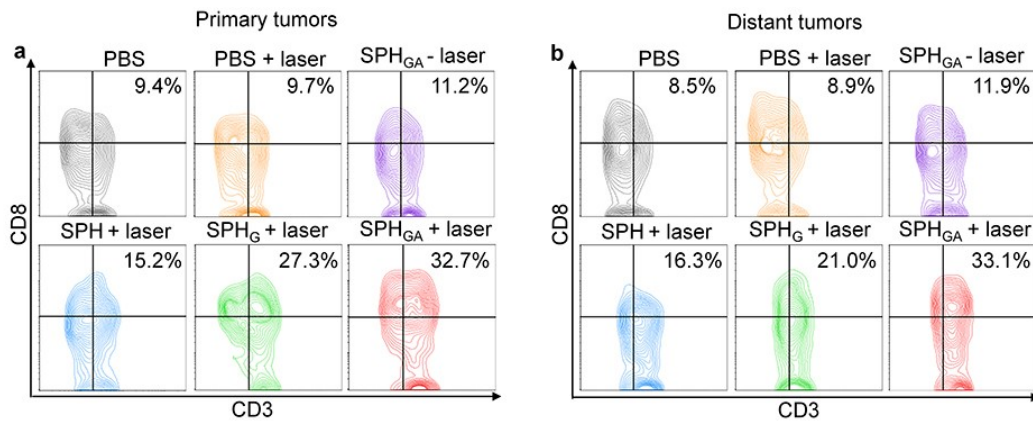


**Fig. S27.** Flow cytometer analysis of CD3<sup>+</sup>CD8<sup>+</sup> T cells in (a) primary tumors and (b) distant tumors after treatments with SPH, SPH<sub>G</sub> and SPH<sub>GA</sub> (250 μg/mL, 200 μL) and laser irradiation (1.0 W/cm<sup>2</sup>, 10 min).

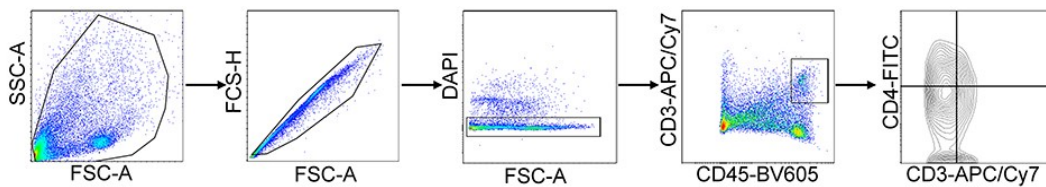


**Fig. S28.** Gating strategy for flow cytometry analysis of matured CD3<sup>+</sup>CD4<sup>+</sup> T cells.

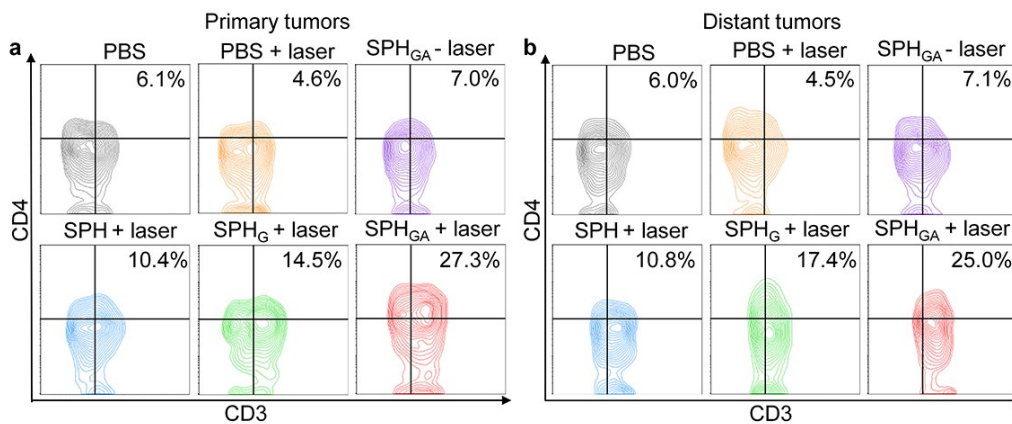


**Fig. S29.** Flow cytometer analysis of CD3<sup>+</sup>CD4<sup>+</sup> T cells in (a) primary tumors and (b) distant tumors after treatments with SPH, SPH<sub>G</sub> and SPH<sub>GA</sub> (250 μg/mL, 200 μL) and laser irradiation (1.0 W/cm<sup>2</sup>, 10 min).

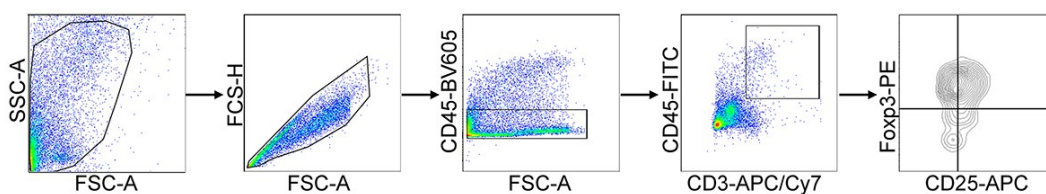


**Fig. S30.** Gating strategy for flow cytometry analysis of T<sub>reg</sub> cells.

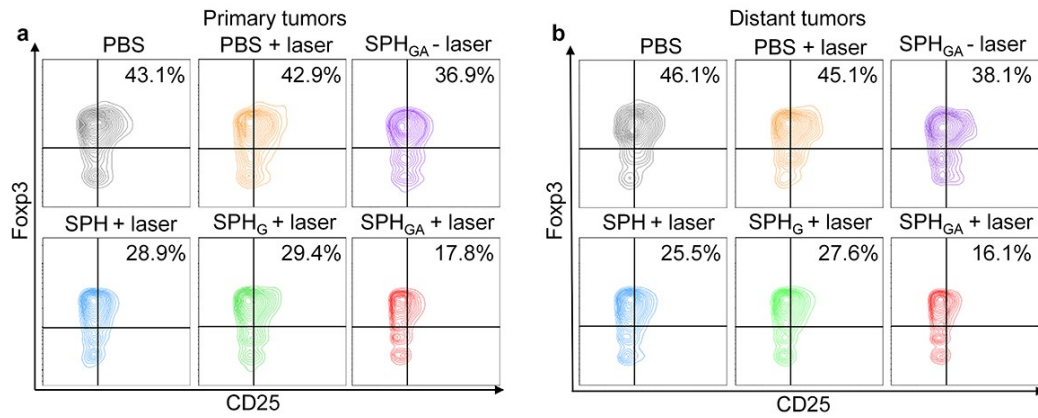


**Fig. S31.** (a) Flow cytometer analysis of T<sub>reg</sub> cells in (a) primary tumors and (b) distant tumors after treatments with SPH, SPH<sub>G</sub> and SPH<sub>GA</sub> (250 µg/mL, 200 µL) and laser irradiation (1.0 W/cm<sup>2</sup>, 10 min).

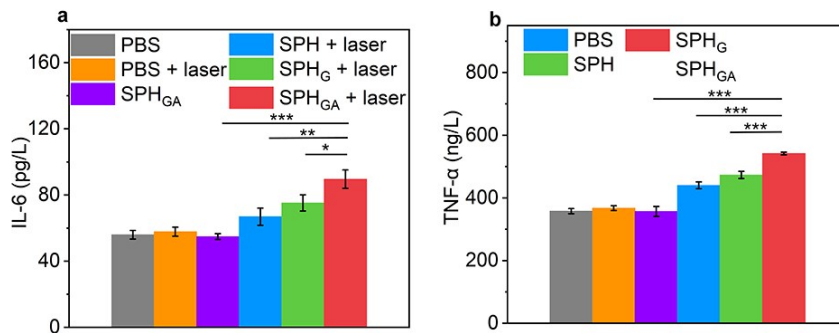


**Fig. S32.** The levels of (a) IL-6 and (b) TNF-α in serum of tumor-bearing mice after treatments with SPH, SPH<sub>G</sub> and SPH<sub>GA</sub> (250 µg/mL, 200 µL) and laser irradiation (1.0 W/cm<sup>2</sup>, 10 min) (n = 5).

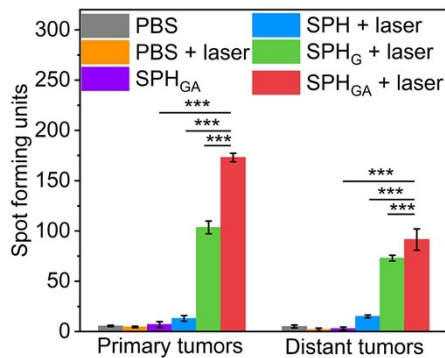


**Fig. S33.** Units of IFN-γ spot in primary tumors and distant tumors after treatments with SPH, SPH<sub>G</sub> and SPH<sub>GA</sub> (250 µg/mL, 200 µL) and laser irradiation (1.0 W/cm<sup>2</sup>, 10 min) (n = 3).